Increased sensitivity in T-ray liquid spectroscopy using rapid sample modulation

Samuel P. Mickan[a], Jesper Munch[b], X.-C. Zhang[c] and Derek Abbott[a]

[a]Centre for Biomedical Engineering, School of Electrical & Electronic Engineering, The University of Adelaide, Australia;
[b]Department of Physics & Mathematical Physics, The University of Adelaide, Australia;
[c]Center for Terahertz Research, Rensselaer Polytechnic Institute, Troy NY, USA.

ABSTRACT

Pulsed THz (T-ray) spectroscopy is a sensitive, non-invasive technique for studying materials from material science to biology, but transmission measurements of liquid samples, especially water, are limited by noise. This paper shows that the accuracy of T-ray material parameter measurements of liquid samples can be greatly increased, especially for highly-absorbing liquids, by using a rapid modulation of the liquid in the T-ray beam path (Differential Time-Domain Spectroscopy), coupled with a novel implementation of mean and amplitude detection. The theoretical calculations are supported by proof-of-principle experiments. Liquid transmission T-ray studies are valuable for understanding solvation dynamics of salts, exploring long-range structure in mixtures and probing biomolecules in suspension.

Keywords: T-rays, terahertz (THz) time-domain spectroscopy, ultrafast photonics, liquid

1. INTRODUCTION

T-rays are unique in their ability to measure certain characteristics of liquids, including the characteristic relaxation times of permanent or induced molecular dipole moments.

Liquid spectroscopy is best carried out with dual-thickness measurements, using a thick sample and a thin sample of the same liquid.[1] This paper proposes making dual-thickness measurements at higher modulation frequencies by rapidly swapping between the thick and thin samples, that is, a novel technique of liquid Differential Time-Domain Spectroscopy (DTDS). Liquid DTDS combines the benefits of: (i) accurate parameter estimation due to dual-thickness measurements, and (ii) reduced noise from double-modulated DTDS.[2] In T-ray studies of liquids and liquid mixtures, the main limitations on accuracy are the fluctuations in T-ray pulse amplitude arising from laser noise (T-ray noise) – the effect of this noise can be reduced by sample modulation (DTDS).

In this paper, liquid DTDS is proposed, modelled and tested. Noise analysis in Sec. 2 shows the potential for improving the accuracy of T-ray measurements of liquids, especially for biologically important high-dielectric constant mixtures containing water. Experiments in Sec. 3 with a prototype sample modulation system based on an audio speaker are used to demonstrate the feasibility of liquid DTDS. The results in Sec. 4 show that liquid DTDS provides the same information as traditional T-ray TDS, but has the potential for far lower noise, and thus increased sensitivity.

1.1. Motivation

The accuracy of estimating the T-ray frequency parameters of fluid samples in dual-thickness T-ray spectroscopy is limited by: (i) fluctuations in the T-ray pulses, caused by laser fluctuations, and (ii) the accuracy of the thickness measurements.[3,4] Noise in the T-ray beam is caused primarily by laser fluctuations, which are known to have a $1/f$ characteristic, that is, the fluctuation amplitude is greater at lower frequencies.[5]

Further author information: Samuel Mickan (corresponding author), Email: samuel.mickan@adelaide.edu.au, Tel: +61.8.8303.4115; Jesper Munch, Email: jesper.munch@adelaide.edu.au; X.-C. Zhang, Email: zhangxc@rpi.edu; Derek Abbott, Email: dabbott@eleceng.adelaide.edu.au

1.2. Previous studies

For infrared and THz spectroscopy, the typical accuracy of measured liquid parameters in the literature to date is to two decimal places, or worse than 0.1%.[6–10] The work in this paper attempts to improve the accuracy of these measurements by two orders of magnitude.

Keiding et al. have studied T-ray spectra of liquid water as a function of temperature, and modelled the spectra using a Debye relaxation model and numerical simulation.[7,11] These experiments were performed using a reflective TIR method. The temperature dependence of liquid water has also been compared to deuterated water D_2O.[12] An alternative model of the T-ray response of liquid water, describing molecular plasma oscillations in an ice-like crystalline lattice, has been proposed from transmission data.[13]

Liquid water shows a very high T-ray absorption, greater than 200 cm^{-1} at 1 THz, whereas nonpolar liquids have coefficients around 100× smaller (for example, benzene, carbon tetra-chloride and cyclohexane).[14] Ref. 8 have studied the temperature dependence of the solvents benzene and toluene, observing rotational and librational bands. Ref. 1 have studied numerous liquids of varying polarity with a dual-thickness sample cell, based on a polyethylene bag held between two movable silicon or polyethylene windows, including water, methanol, 1-propanol and liquid ammonia. A number of optical-pump and T-ray-probe studies have explored the response of solvents and dyes to photoexcitation,[15] and linked these results to finite difference time-domain models.[16] The solvation dynamics of polar and nonpolar liquids, including acetonitrile and water,[17] acetone, acetonitrile and methanol[9] and water,[18] have been related to molecular dynamics simulations to explore the relationship of decreasing T-ray absorption with increasing liquid structure.[19] The solvation dynamics of lithium salts in water, methanol and propylene carbonate have been explained with Debye relaxation models.[10]

The experiments in this paper use a dual-thickness geometry, where the sample and reference waveforms are measured through thick and thin versions of the sample respectively. Dual-thickness geometry systems have been used by Ref. 1 and Ref. 4.

1.3. Objective summary

This paper shows that double-modulated DTDS can be used to reduce the noise in fluid parameter measurements. In a typical T-ray transmission spectrometer with a SNR of 100:1, each time-domain measurement takes approximately 5 mins, and noise is dominated by laser fluctuations. By rapidly modulating the sample, and simultaneously measuring the reference and sample waveforms (*amplitude and mean detection*), the time between measuring the sample and reference waveforms can be reduced to a time determined by the speed of the modulator. Therefore only one delay scan is required to sample both T-ray waveforms, and the time delay between each sample and reference measurement is the inverse of the modulation frequency. For a 10-Hz modulation speed, the increase in effective modulation frequency is 3000 times, and the corresponding decrease in the noise amplitude is 3000 times.

2. LIQUID DTDS THEORY

For liquid spectroscopy using a dual-sample geometry, the accuracy of parameter estimation depends on T-ray noise and the accuracy of the thickness change (translation stage noise). This section quantifies the benefits of double-modulated DTDS for characterising two classes of liquids: those with a low T-ray absorption (for example, the solvent 1,4-dioxane) and those with a high T-ray absorption (for example, water). The aim is to measure material parameters with an accuracy better than 10^{-4}.

2.1. Dual-sample theory

In T-ray spectroscopy, the T-ray pulse is modelled as a spectrum of Fourier components, propagating as a plane wave through the sample.

The simplest and most common geometry for free-space T-ray TDS is transmission through an orthogonally-positioned slab of homogeneous material, characterised by $\tilde{n}_s$. This slab may be free-standing in air, or either deposited on or implanted into a substrate or holder. The model for the normalised sample spectrum depends on each individual experiment, but three main classes can be discerned: (i) thick samples, (ii) thin samples, and (iii) dual-thickness samples.

A thick sample is a slab that causes sufficient delay so that the transmitted pulse can be measured without any overlap with the first Fabry-Pérot (FP) reflection. The exact requirements for the delay will depend on the desired total scan length.[20] A diagram of a thick sample and the reference and sample paths is shown in Fig. 1. Note that the substrate material both before and after the sample must also be sufficiently thick to avoid any FP reflections in the measured pulses. Thin substrates are discussed below with thin samples.

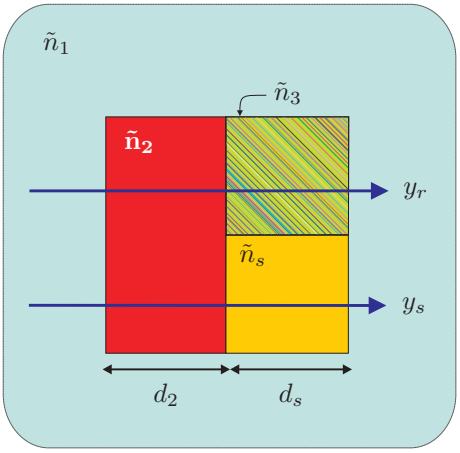

Figure 1. T-ray transmission notation for a single-thickness sample. This schematic shows the notation for modelling T-ray propagation through a sample slab, mounted on a substrate. The sample to be studied, with refractive index $\tilde{n}_s$, is attached to a substrate material with refractive index $\tilde{n}_2$, and both are immersed in a medium of refractive index $\tilde{n}_1$. The green area, $\tilde{n}_3$, typically has a refractive index equal to $\tilde{n}_1$ or to $\tilde{n}_2$, depending how the sample is prepared: if the sample is implanted into the substrate, $\tilde{n}_3 = \tilde{n}_2$. If the sample is deposited onto the substrate, then $\tilde{n}_3 = \tilde{n}_1$. In single-thickness measurements, the reference pulse y_r passes through the substrate then the green area. The spectral components of the waveforms are determined by FFT, $\tilde{S}_s = \mathcal{FT}(y_s)$ and $\tilde{S}_r = \mathcal{FT}(y_r)$.

In the thick sample geometry, the experimentally-measured spectral components of the reference and sample pulses can be modelled by

$$\tilde{S}_r = A(\omega) \cdot t_{12} \cdot p_2 \cdot t_{23}, \qquad \tilde{S}_s = A(\omega) \cdot t_{1s} \cdot p_s \cdot t_{s3} \tag{1}$$

where $A(\omega)$ is a factor representing all other system responses that remain constant between the sample and reference measurements. Thus an experimental transmission ratio $\tilde{T}$ can be measured that has a complex amplitude and phase at all frequencies,

$$\tilde{T} = \frac{\tilde{S}_s}{\tilde{S}_r} = \rho \cdot e^{-j\phi}. \tag{2}$$

Using the equations for plane wave propagation and reflection,[21] the sample refractive index n_s can be determined from the other refractive indices (in Fig. 1), the sample thickness and the transmission ratio $\tilde{T}$,

$$\frac{\tilde{n}_s(\tilde{n}_1 + \tilde{n}_2)(\tilde{n}_2 + \tilde{n}_3)}{\tilde{n}_2(\tilde{n}_1 + \tilde{n}_s)(\tilde{n}_s + \tilde{n}_3)} \cdot e^{-j(\tilde{n}_s - \tilde{n}_2)\omega d/c_0} = \tilde{T}. \tag{3}$$

This set of equations can be solved for the real and imaginary parts of $\tilde{n}_s$ using iterative techniques.[22]

For the common case where the sample $\tilde{n}_s$ is placed in a vacuum or air, $\tilde{n}_1 = \tilde{n}_2 = \tilde{n}_3 = 1.0$, a simplified expression can be determined for the transmitted pulse (and any time-separated FP pulses).[23] For a sample with very low T-ray absorption, that is $\kappa_s \ll n_s$, analytic expressions for n_s and κ_s can be written in terms of the magnitude ρ and phase ϕ of the transmission ratio T,

$$n_s = \phi \cdot \frac{c_0}{\omega d} + 1, \qquad \kappa_s = \ln\left(\frac{4n_s}{\rho \cdot (n_s + 1)^2}\right) \cdot \frac{c_0}{\omega d}. \tag{4}$$

An even simpler transmission geometry can be constructed of two thicknesses of the same material, as shown in Fig. 2. A dual-thickness measurement greatly simplifies modelling. Figure 2 shows the propagation of radiation through the sample, of complex refractive index $\tilde{n}_2$, and across two interfaces between the sample and the surrounding medium (air), $\tilde{n}_1 \approx 1.0$. The simple equations used for estimating the material parameters are derived from the equations for Fresnel transmission and reflection at interfaces.

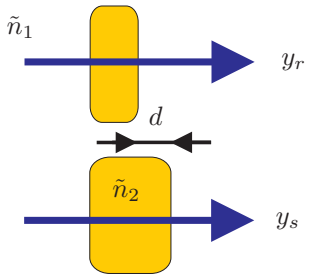

Figure 2. Dual-thickness parameter estimation geometry. Waveforms y_s and y_r are measured having respectively passed through the thick (sample) and thin (reference) samples. The spectral components of the waveforms are determined by FFT, $\tilde{S}_s = \mathcal{FT}(y_s)$ and $\tilde{S}_r = \mathcal{FT}(y_r)$. The difference in thickness between the two measurements is denoted d.

The ratio of the transmission spectra $\tilde{S}$ can be entirely determined in terms of refractive indices and the sample thickness,

$$\frac{e^{-j\tilde{n}_2\omega d_{\text{thick}}/c_0}}{e^{-j\tilde{n}_2\omega d_{\text{thin}}/c_0}e^{-j\tilde{n}_1\omega(d_{\text{thick}}-d_{\text{thin}})/c_0}} = \tilde{T}, \tag{5}$$

where $\tilde{n}_1$ is the material that replaces the space taken up by the extra thickness of the thick sample, typically air.

Equation (5) simplifies to

$$\exp(-j\omega/c_0 d(\tilde{n}_2 - 1)) = \tilde{T}, \tag{6}$$

where $d = d_{\text{thick}} - d_{\text{thin}}$ and $\tilde{n}_1 = 1$. Since $\tilde{T}$ is complex, $\tilde{T} = \rho e^{j\phi}$, and $\tilde{n} = n - j\kappa$,

$$\exp(-\omega d\kappa/c_0) = \rho, \qquad \omega d(n_2 - 1)/c_0 = \phi, \tag{7}$$

where the complex refractive index $\tilde{n} = n - j\kappa$, d is the thickness change of the sample, c_0 is the speed of light in a vacuum.

The material parameters can then be extracted by rearranging the above equations,[24]

$$n = \frac{-\phi\ c_0}{\omega d} + 1, \qquad \kappa = -\ln(\rho)\frac{c_0}{\omega d}. \tag{8}$$

These calculations provide a value for the T-ray refractive index n and extinction coefficient κ of the mixture. The absorption coefficient, α is related to the extinction coefficient through the equation $\alpha = 2\omega\kappa/c_0$. The values of $\tilde{S}_s$ and $\tilde{S}_r$ can be measured by taking the Fourier transform of the transmitted time-domain T-ray pulses, y_s and y_r respectively.

2.2. Noise sources

The accuracy of Eq. (8) depends only on the noise of the T-ray spectrometer, $\delta\phi$ and $\delta\rho$, and on errors in the translation stage measurement δd. The influence of errors on the parameter of interest ($\tilde{n}$) can be estimated using:

$$\delta n = \delta n_d + \delta n_\phi, \qquad \delta\kappa = \delta\kappa_d + \delta\kappa_\rho, \tag{9}$$

where the error contributions are calculated using the partial derivatives:

$$\delta n_d = \frac{\partial n}{\partial d}\,\delta d = \frac{\phi\ c_0}{\omega}\ \frac{1}{d^2}\ \delta d, \qquad \delta\kappa_d = \frac{\partial\kappa}{\partial d}\delta d = \frac{\ln(\rho)\ c_0}{\omega}\ \frac{1}{d^2}\ \delta d, \tag{10}$$

$$\delta n_\phi = \frac{\partial n}{\partial\phi}\,\delta\phi = -\frac{c_0}{\omega d}\,\delta\phi, \quad \& \quad \delta\kappa_\rho = \frac{\partial\kappa}{\partial\rho}\delta\rho = -\frac{c_0}{\omega d}\ \frac{\delta\rho}{\rho}. \tag{11}$$

Using Eq. (7), and the relations for uncorrelated noise sources ($\langle\delta n^2\rangle = \langle\delta n_d^2\rangle + \langle\delta n_\phi^2\rangle$, $\langle\delta\kappa^2\rangle = \langle\delta\kappa_d^2\rangle + \langle\delta\kappa_\rho^2\rangle$), expressions for the uncertainty in measurements due to phase, amplitude and thickness uncertainties can be

obtained:

$$\delta n = \frac{n-1}{d}\sqrt{(\frac{2\ c_0\ \delta\phi_r}{\omega(n-1)})^2+(\delta d)^2}, \tag{12}$$

$$\delta\kappa = \frac{\kappa}{d}\sqrt{(\frac{\sqrt{2}\ c_0}{\omega\kappa}\cdot\frac{\delta\rho_r}{\rho_r})^2+(\delta d)^2}. \tag{13}$$

The errors due to the translation stage are proportional to $\delta d/d$. The errors due to T-ray noise are proportional to $\delta\phi/d$ for n and $\delta\rho/(\rho d)$ for κ. The aim is to minimise the effects of noise on the parameter measurements.

2.2.1. Translation stage noise

Translation stage noise δd arises due to uncertainty about the thickness change of a sample d. The effect of translation stage noise can be minimised by designing experiments with a small ratio of δd to d.

For noise dominated by errors in d, T-ray noise is neglected, thus Eqs. (12) and (13) can be simplified by ignoring the first term in the square root, giving

$$\delta n = (n-1)\frac{\delta d}{d}, \qquad \delta\kappa = \kappa\frac{\delta d}{d}. \tag{14}$$

Equation (14) indicates that noise can be reduced by using a large thickness change d compared to the thickness measurement error δd. The value of δd is limited by the resolution of the actuator controlling the sample thickness.

The measurement of thickness change d can be extremely accurate, better than 1:10^4, using closed-loop feedback control of the mechanism used for changing the sample thickness. An accuracy of $\frac{\delta d}{d} < 10^{-4}$ can be achieved by using, for example, a 5-mm distance change between thicknesses and 0.4-μm stage resolution, or a 30-μm piezoelectric stage with 1-nm resolution (see Sec. 5). An accuracy of 10^{-4} would constitute an improvement of 100 times over most T-ray liquid characterisation results.

When $\delta d/d$ is less than 10^{-4}, the contribution of translation stage noise to the experimental measurements can be neglected in comparison to errors caused by noise in the T-ray beam.

2.2.2. T-ray system noise

The T-ray noise is typically the dominant source of noise in T-ray experiments, and comes from three main sources: (i) the T-ray emitter, (ii) the T-ray detector, and (ii) the probe beam. The combined noise of the emitter and detector dominates and is multiplicative, that is, proportional to the signal strength: a time-domain plot of T-ray noise is shown in Fig. 3 as fluctuations in the peak of a T-ray pulse. The noise in the probe beam is additive, that is, independent of signal strength, and only dominates when the signal strength is low.[20]

T-ray noise arises from fluctuations in the power and alignment of the pump laser beam – as the alignment and power change, the intensity of the generated T-rays and the efficiency of the T-ray detector both fluctuate. In experiments, it turns out that amplitude of the T-ray fluctuations is proportional to the measured T-ray amplitude; this can be understood by considering that at peak T-ray powers, the alignment is critical and is easy to disturb. For zero T-ray power, when the T-ray beam is completely blocked, there is no T-ray noise – in this case, the noise is due to fluctuations in the probe beam. Probe beam noise is independent of the T-ray power and depends on the characteristics of the laser itself. These two sources of noise both contribute to errors in T-ray measurements, but each source tends to dominate in different situations.

T-ray noise has a $1/f$ spectrum, as shown in Fig. 4. Normally the two measurements required for material characterisation are measured over a period of minutes, and during this time the fluctuations due to T-ray noise can be large: $1/f$ noise generates larger fluctuations over longer times. However, by taking the reference and sample measurements, required in T-ray spectroscopy, at a higher speed, the fluctuation in laser power between measurements can be reduced. Rapid sample modulation, dubbed T-ray Differential Time-Domain Spectroscopy (DTDS), has previously been used on solid thin films[2] and biosensor slides,[25] but not on liquid or gas samples.

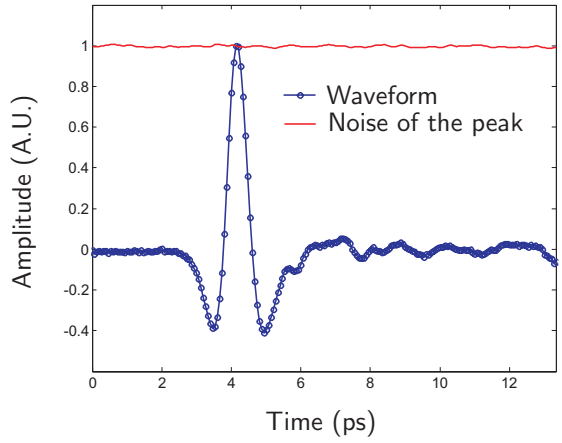

Figure 3. Measured T-ray waveform, and peak fluctuation. This graph shows in blue a T-ray waveform measured over about 5 minutes with the T-ray spectrometer used for the experiments in this paper (Sec. 3). The peak of this waveform fluctuated over time, as shown by the red plot in this Figure, giving an estimation of the noise, or inaccuracy, in the waveform measurement. This peak fluctuation represents the main source of noise in T-ray measurements not limited by absorption. The fluctuation has a spectral distribution shown in Fig. 4. Each of the plots comprises 201 points. The measurements were made with a LIA time constant of 100-ms.

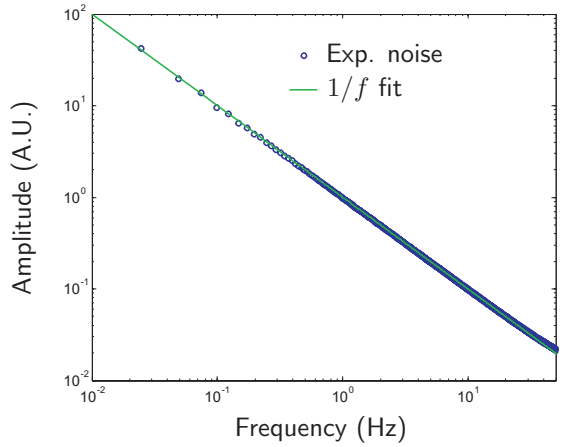

Figure 4. Experimental T-ray noise spectrum. This measured plot shows the $1/f$ trend of T-ray noise. The experimental spectrum, shown as blue circles, was calculated using a numerical FFT from a set of time-domain measurements of the peak of the T-ray pulse, partially shown in Fig. 3. The experimental spectrum fits very closely to a $1/f$ relationship, shown as a green line, over the available measurement frequency range. The 8,192 time-domain samples were taken with a time spacing of approximately 5 ms, giving a sample time of 41 s and a measurement frequency range of approximately 0.024 to 100 Hz. Using liquid DTDS instead of normal T-ray TDS would decrease the drift time from approximately 5 mins to 0.05 s (0.003 Hz to 50 Hz), theoretically decreasing the noise caused by laser fluctuations by up to 4 orders of magnitude.

2.3. The effect of noise on measurements

The best modulation system for liquid spectroscopy turns out to depend on the properties of the liquid. For a low-κ liquid, a high accuracy can be achieved by using a very large thickness change up to $d = 10$ mm. For a high-κ liquid, only a small thickness change is possible, and the errors must be reduced in two ways: (i) the thickness change must be accurate, for example, by using a piezoelectric translator, and (ii) the inherent noise in the T-ray signal must be reduced, by using for example high-frequency sample modulation in double-modulated DTDS.

For dioxane measurements (low κ), an accuracy of approximately 10^{-4} is desirable, thus from Eq. (19), a thickness change of approximately 10 mm is required, with a resolution of 1 μm. Since dioxane has low absorption, this is possible. For water measurements (high κ), a thickness of 1 cm is unusable since the T-ray absorption is too high. A thickness change of approximately 100 μm and a resolution of 10 nm is required, using for example a piezoelectric actuator.

For experiments dominated by multiplicative noise, that is, noise due to fluctuations in the T-ray signal (pump beam) rather than noise in the detection system (probe beam),[26] the phase error is approximately equal in both the sample and reference spectra,

$$\delta\phi_s \approx \delta\phi_r.$$

From $\phi = \phi_s - \phi_r$ and Eq. (2.3), $\delta\phi \approx 2\delta\phi_r$.

For uncorrelated amplitude noise in both the sample and reference, the combined effect of noise in both

sample and reference can be estimated from

$$\frac{\langle \delta\rho^2 \rangle}{\rho^2} = \frac{\langle \delta\rho_r^2 \rangle}{\rho_r^2} + \frac{\langle \delta\rho_s^2 \rangle}{\rho_s^2}. \tag{15}$$

For multiplicative noise, the relative amplitude error is similarly approximately equal in both the sample and reference spectra, giving

$$\frac{\delta\rho}{\rho} \approx \sqrt{2}\frac{\delta\rho_r}{\rho_r}, \tag{16}$$

$$\delta\rho = \frac{\sqrt{2}\exp(\frac{-\omega d\kappa}{c_0})}{\rho_r}\ \delta\rho_r. \tag{17}$$

For T-ray noise dominated measurements, Eqs. (12) and (13) can be simplified by ignoring the small second term in the square root, giving

$$\delta n = \frac{2\ c_0\ \delta\phi_r}{\omega\ d}, \qquad \delta\kappa = \frac{\sqrt{2}\ c_0}{\omega\ d} \cdot \frac{\delta\rho_r}{\rho_r}. \tag{18}$$

That is, the errors are inversely proportional to the thickness change, and proportional to $\delta\phi_r$ (for n) the ratio of $\delta\rho_r/\rho_r$ (for κ). This equation provides a good estimate of noise sources in the final measurements, and is verified experimentally in Sec. 4.2.

These equations can be understood by substituting approximate values from a typical T-ray spectrometer measurement. A typical measurement could have, for example, $\omega = 6.3 \times 10^{12}$ rad/s at a frequency of 1 THz, and $\rho_r = 0.655$, $\delta\rho_r = 0.015$ and $\delta\phi_r = 0.025$ rad for a scan of the organic solvent 1,4-dioxane, using the liquid T-ray spectrometer described in Sec. 3. In this measurement, the LIA time constant was 100 ms, giving a scan duration of approximately 5 mins. Using the numbers in this example,

$$\delta n \approx \frac{5 \cdot 10^{-6}}{d}, \qquad \delta\kappa \approx \frac{3 \cdot 10^{-6}}{d}. \tag{19}$$

From Eq. (19) it can be seen that an accuracy of 10^{-4} is achievable at this noise level (100-ms LIA time constant and 5 min scan) by using an approximate thickness change of $d > 10$ mm. This large thickness change is possible with large volumes of liquid with a low T-ray absorption. If, however, the T-ray absorption of the liquid is not very low, a 50-mm-thick sample will attenuate the T-rays too greatly to be detected. For high-κ samples, for example water, the initial noise in the T-ray signal must be reduced to compensate for the necessity of a small thickness change.

For high-κ samples, $\tilde{S}_s$, is greatly attenuated, and $\delta\rho$ is dominated by additive noise.

Thus

$$\delta\kappa = \frac{\sqrt{2}\ c_0}{\omega\ d} \cdot \frac{\delta\rho_s}{\exp(\frac{-\omega d\kappa}{c_0})}, \tag{20}$$

$$\approx \frac{1.3 \cdot 10^{-4}}{d}\ \delta\rho_s\ \frac{1}{\rho}. \tag{21}$$

The error is proportional to $1/\rho$.

The influence of increasing the modulation thickness, d, on the accuracy of our estimations when using two different example liquids, dioxane ($\kappa_{\text{dioxane}} = 0.013$) and water ($\kappa_{\text{water}} = 0.478$). The graph in Fig. 5 shows that the error in κ decreases with increasing thickness, from the first term in Eq. (21), until a maximum thickness is reached, beyond which the error begins to increase again, due to attenuation of the T-ray signal in the sample, shown as the second term in Eq. (21). The thickness d that corresponds to a minimum error depends on the T-ray absorption coefficient of the liquid sample (κ).

Figure 5 shows that a thickness change of even 1 mm generates a very high error in a high-κ liquid, thus limiting experiments to sub-mm modulation.

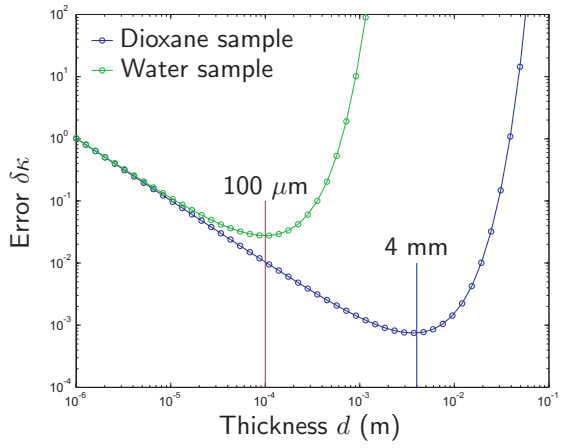

Figure 5. Calculated $\delta\kappa$ as a function of sample thickness. This plot shows the relationship of measurement error $\delta\kappa$ to the thickness change of the sample d in dual-thickness T-ray material characterisation (see diagram in Fig. 2). The two liquids represented in the graph are dioxane, $\kappa = 0.013$, and water, $\kappa = 0.478$. For the typical noise in a T-ray spectrometer, for example $\delta\rho_s = 0.015$ (error in real part of measured sample spectrum $\tilde{S}_s$), the error in the estimation of κ depends on the thickness change of the sample. The error decreases for thicker samples, from Eq. (20), but for highly-absorbing liquids, such as water, the increased thickness attenuates the T-ray signal to a large degree. The vertical lines show the approximate thickness change desirable for minimum error. For dioxane (low κ), a thicker sample is desirable, approximately 4 mm. For water (high κ), the thickness change is much less, approximately 100 μm.

2.4. Noise cancellation: Liquid DTDS

Liquid Differential Time-Domain Spectroscopy (DTDS) relies on the principle of measuring two waveforms (y_r and y_s) at approximately the same time, rather than minutes apart. This is similar to thin film DTDS, which has a good noise performance for small differences between the reference and sample waveforms.[2] However, in liquid DTDS the reference and sample waveforms may differ significantly, undermining the one of the assumptions in thin-film DTDS (that is, $y_r \approx y_s$) so the two waveforms must be measured separately and at approximately the same time. This can be achieved using amplitude and mean detection.

2.4.1. Amplitude & Mean Detection

Amplitude and mean detection is an electronic technique that enables the simultaneous measurement of both the sample and reference waveforms, y_s and y_r, when a sample is modulated in the T-ray beam. Amplitude and mean detection can be used in any double-modulated DTDS experiment and is implemented as part of the signal detection electronics. In amplitude and mean detection, instead of discarding 50% of the y_d waveform as in double-modulated DTDS, half the signal is used to simultaneously measure y_r. The hardware requires no modification from double-modulated DTDS, and the time between measuring y_d and y_r is reduced from the order of minutes to the order of milliseconds. For measurements dominated by $1/f$ noise, a reduction in the scan-to-scan delay time increases the SNR, potentially by several orders of magnitude.

Conceptually, mean and amplitude detection can be implemented in stand-alone electronics, using for example a fast analog-to-digital converter ($\gg f_1$) and two stages of digital demodulation, synchronised with the movement of the delay stage. The diagram in Fig. 8 shows schematically how the double-modulated signal from the T-ray system is demodulated in two stages.

The double demodulation process can be understood in the time domain by looking at the square waveform detected by the photodiodes as the sample is modulated differentially. A model of the waveform current that would be detected by the photodiodes is shown in Fig. 6. The sketch includes indications of the relationships between the mean and amplitude waveforms (y_m and y_a respectively) and y_s and y_r, which are measured at the output of the first mixer (see Fig. 7).

The relationship in Fig. 6 shows that the sample and reference waveforms can be calculated from the amplitude and mean as follows:

$$y_s = y_m - y_a, \qquad y_r = y_m + y_a. \tag{22}$$

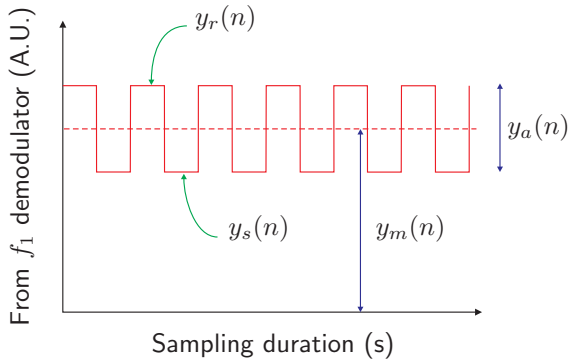

Figure 6. Amplitude and mean detection at one delay point: model. This sketch models the output of the f_1 demodulator, shown in Fig. 8, being modulated by the sample modulation (for example, by repeatedly changing between two liquid sample thickness). This is the time-domain waveform seen for the nth step of the delay stage. The relationship between y_m, y_a, y_s and y_r can be seen in the diagram. Errors arising from amplitude and mean detection are caused by deviations of the observed signal from an ideal square wave, and this depends on the physical constraints of the system, as discussed in Sec. 2.2.

Note that the factors of 2 are missing in Eq. (22) because y_r and y_s are effectively halved by dithering the sample – double modulation causes a 50% reduction in the T-ray signal.[27] The trade-off is a 50% reduction in the signal level for measuring y_r and y_s simultaneously.

3. EXPERIMENT

This Section describes an initial experimental verification of the accuracy of liquid DTDS and discusses its limitations.

The experimental implementation of liquid DTDS involved three main elements: (i) a standard T-ray transmission spectrometer, (ii) a sample holder for modulating the liquid sample at a modulation frequency f_2, and (iii) electronic signal processing to extract the sample and reference waveforms, y_s and y_r. The spectrometer used in these experiments is similar to that in Ref. 4.

The sample holder was required to provide a rapid transition between a thick and thin sample, corresponding to y_s and y_r in dual-thickness spectroscopy. In the prototype system this was implemented using one large fixed Teflon window and one moving window mounted on an audio speaker. The speaker was driven by a square wave to switch rapidly between the thick and thin positions. The signal processing consisted of two parts: the standard DTDS double de-modulation to extract the difference waveform $y_d = y_s - y_r$, and a second part to measure the mean waveform $y_m = y_s + y_r$.[2] *Amplitude and mean detection* is described in Sec. 3.1 below.

The two Teflon windows, mounted perpendicular to the T-ray beam axis, were thicker than 10 mm to avoid Fabry-Pérot reflections in the recorded waveform. Teflon is a good material for T-ray windows because of its low refractive index and low absorption. The actual liquid samples are held in an high-density polyethylene (HDPE) bag, a material that does not dissolve in the solvent. HDPE has a low T-ray refractive index and low T-ray absorption. With an average wall thickness less than 0.1-mm thick, less than the majority of T-ray wavelengths, and a very low refractive index mismatch between Teflon and HDPE, etalon effects from the plastic bag walls were negligible. Experimentally, no multi-reflections were observed in the measured pulses.

For a liquid in the HDPE bag undergoing rapid movement, when the Teflon walls move apart, it is important that no bubbles form in the liquid itself due to the drop in pressure. The process by which bubbles form spontaneously in a liquid is generally called cavitation. Cavitation occurs in a liquid if the local pressure drops below the vapour pressure of the liquid.[28] Each bag was at least 50% filled with air, thus any increase in volume between the Teflon plates was compensated for by a decrease in air pressure, rather than a change in the pressure of the liquid by any large amount. No bubbles formed, and sufficient liquid was in the bag, so gaps were being filled by liquid pulled into the increasing volume.

3.1. Amplitude and mean detection

Amplitude and mean detection can be realised with an anti-aliasing filter, a local oscillator referenced to f_1, a local oscillator referenced to f_2 and an integrator, as shown in Fig. 7.

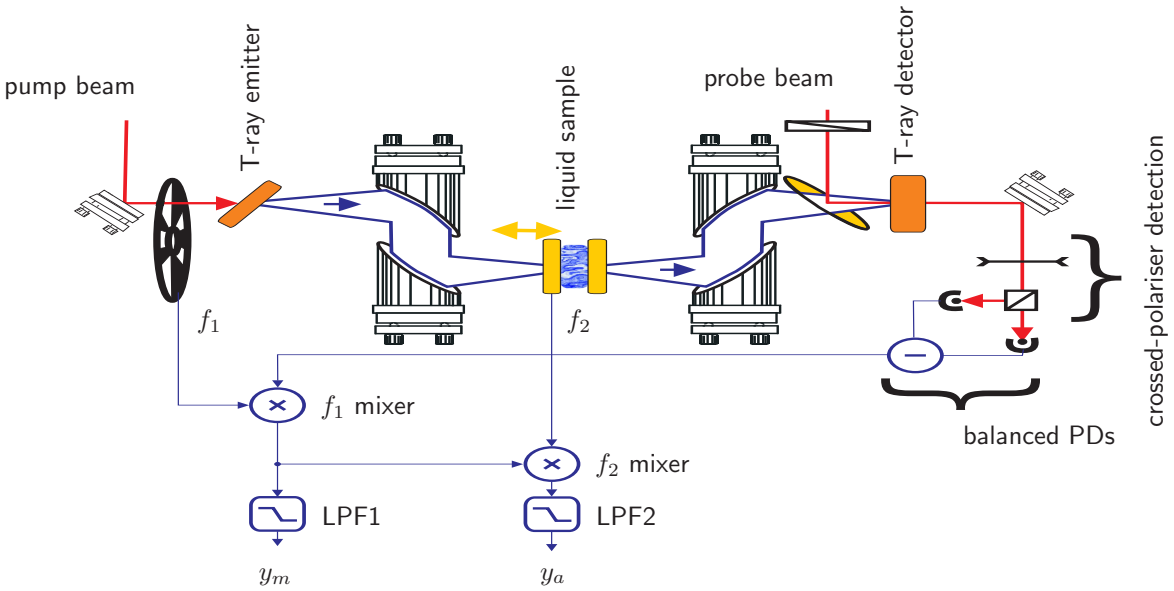

Figure 7. DTDS spectrometer configured for amplitude and mean detection. This schematic describes a T-ray spectrometer with a liquid DTDS sample holder. The standard spectrometer elements are described in.[29] The experimental system is the same as for standard liquid spectroscopy,[4] however this Figure also shows the electronics used in amplitude and mean detection (described in Sec. 3.1). The optical chopper wheel modulates the T-ray beam at frequency f_1 with an on-off square wave signal, then the sample holder imparts an additional modulation at frequency f_2. The T-ray signal is detected using the crossed polarisers and balanced photodiodes, then demodulated in two stages by mixing with electronic oscillators f_1 and f_2. The phase on these local oscillators is locked to the physical modulators. By low-pass filtering the outputs of the two mixers, the values of y_m and y_a can be measured at each delay stage point, as shown in the time-domain in Fig. 6.

In the experimental work in this paper, the system was implemented with three LIAs (Lock-in Amplifiers), as shown in Fig. 8. The same effect could be achieved digitally with a low-noise preamplifier, a fast analog-to-digital converter and a dedicated processor.

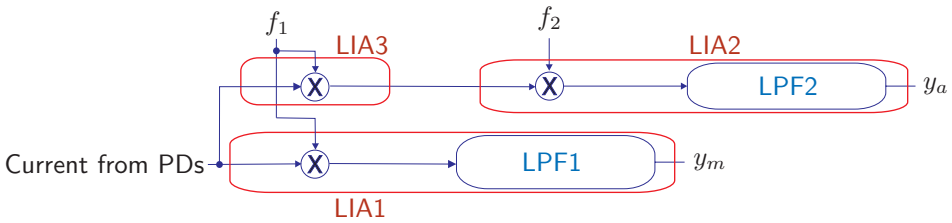

Figure 8. Schematic of mean and amplitude detection. This block diagram shows the signal processing steps required to extract the y_m and y_a waveforms from the balanced photodiode current. The blocks are shown implemented with LIAs, as in the experimental Section of this paper, Sec. 4. The double-modulated signal from the balanced photodiodes (PDs) is demodulated in two stages. The first demodulation by the higher frequency f_1 is performed by the third LIA. The output of this first demodulator is shown as the square waveform in Fig. 6. The first LIA performs the same demodulation, then uses an in-built Low-Pass Filter (LPF), 'LPF1', to output the mean of the modulated waveform. The first LIA is part of the normal noise reduction of T-ray TDS: the mechanical chopper provides an AC signal that is detected by the first LIA, which smooths out any other modulation. The second demodulation by the low frequency f_2 in the second LIA is followed by a narrow band 'LPF2'. Experimentally, the bandwidth of the LPFs are determined by the time constants of the LIAs. The third LIA acts as the f_1 demodulator, with a short time constant (approximately 30 μs), and the second LIA acts as the f_2 demodulator with a long time constant (approximately 100 ms).

4. RESULTS

The results for a preliminary demonstration of liquid DTDS show that liquid spectroscopy is functional, and show the technique's limitations. The difference waveform y_d was shown experimentally to be equal to $y_r - y_s$, as required for the DTDS analysis. The accuracy of the measurements, which is critical to accurate sample characterisation, was shown to depend on the static linearity of the actuator (audio speaker), the dynamic non-linearities introduced at higher modulation frequencies and larger modulation amplitudes. The goal in a liquid DTDS system is to have as large a movement as possible at as high a frequency as possible. A large movement (thickness change d) increases the accuracy of the parameter estimation (see Sec. 2). A higher modulation frequency reduces $1/f$ noise in the final result – this is due to the nature of $1/f$ noise, where larger fluctuations occur over longer time scales than the short modulation period. The best possible modulation amplitude and frequency depends on the mechanical limitations of the sample holder, as seen in the following results.

4.1. Test of amplitude & mean detection

Figure 9 shows the results of an experimental test of mean and amplitude detection in the T-ray spectrometer. The mean and amplitude waveforms were measured as shown in Fig. 8, that is, the outputs of the 2nd and 3rd LIAs respectively. The accuracy of the technique was confirmed by comparing the calculated waveforms, from y_r-calc $= y_m - y_a$ and y_s-calc $= y_m + y_a$ using amplitude and mean data, to two waveforms measured using normal T-ray TDS, y_r-exp and y_s-exp. The slight difference between y-calc and y-exp in Fig. 9 was due to the sample being modulated by an imperfect square wave. This was a mechanical error introduced by the prototype mechanical sample modulation arm, that is the galvanometer.

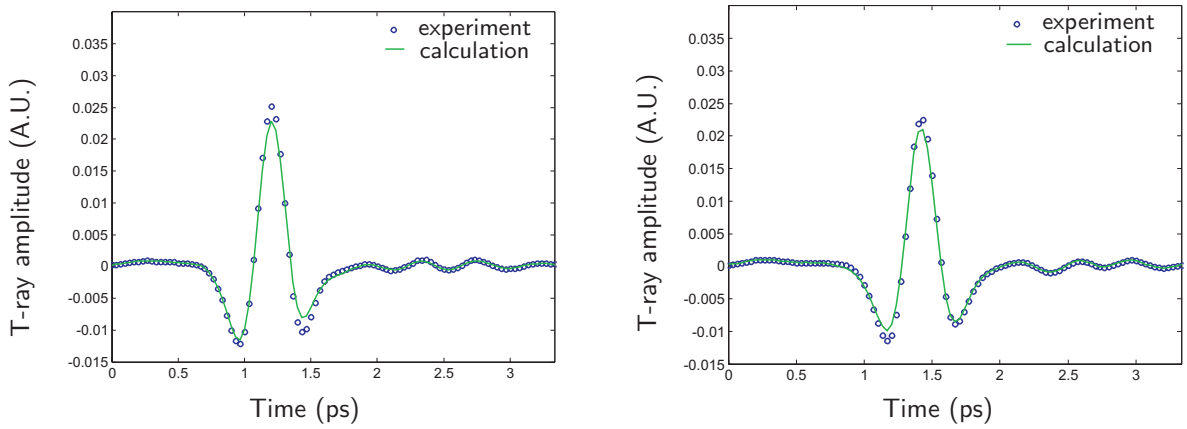

(a) y_r (b) y_s

Figure 9. Measured amplitude and mean detection waveforms. These waveforms are an example of single-scan DTDS. The waveforms y_m and y_a were measured with double-modulated DTDS, using the system shown in Fig. 8. The 'y-calc' waveforms were calculated from $y_r = y_m - y_a$ and $y_s = y_m + y_a$. 'y_r-exp' and 'y_s-exp' were measured using the same T-ray spectrometer and sample, but without modulating the sample and taking two separate sample and reference scans (normal T-ray TDS). The match between 'y-calc' and 'y-exp' is an experimental confirmation that amplitude and mean detection provides exactly the same information about a sample as normal T-ray TDS, but with a potentially far lower noise level.

4.2. Test of the error equations

To confirm the equations of Sec. 2.2, this Section describes the experimental repeatability and estimated uncertainty in actual dual-thickness experiments. Six T-ray TDS measurements of anhydrous dioxane were taken and the standard deviation was estimated using MATLAB. Then Eq. (19) was used to calculate the predicted uncertainty. The calculated uncertainty spectra for estimates of n and κ are shown in Fig. 10. The actual uncertainty in a series of measurements can be estimated from the standard deviation of a series of estimated values of n and κ. The equations provide an accurate estimate or an over-estimation of the error. These results confirm the accuracy of the equations used above to quantify the sources of uncertainty.

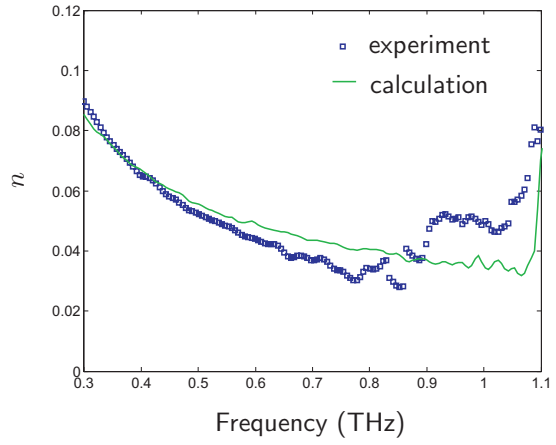

Figure 10. Test of the error equations. This Figure compares: (i) the experimentally-determined standard deviation of six measurements, to (ii) the calculated standard deviation that would be expected from the uncertainty analysis in Sec. 2.2. The experimental uncertainty is the standard deviation function from six repeated experimental measurements (using MATLAB). The dots, calc. represent the standard deviation of the estimated values. The calculated line represents Eq. (19). The example shown is for a liquid sample of anhydrous dioxane. This Figure shows that, for the three liquids shown, the equations provide an accurate estimate or an over-estimation of the error, thus confirming the accuracy of the equations used to quantify the sources of uncertainty in Sec. 2.2.

4.3. Test of liquid DTDS accuracy

Figure 11 shows a direct comparison of the waveforms from double-modulated DTDS (y_d) and normal TDS with the optimal settings described in Sec. 4.4 (1.6 mm modulation displacement at 10 Hz). The large overlap of the waveforms experimentally verifies the principle of liquid DTDS.

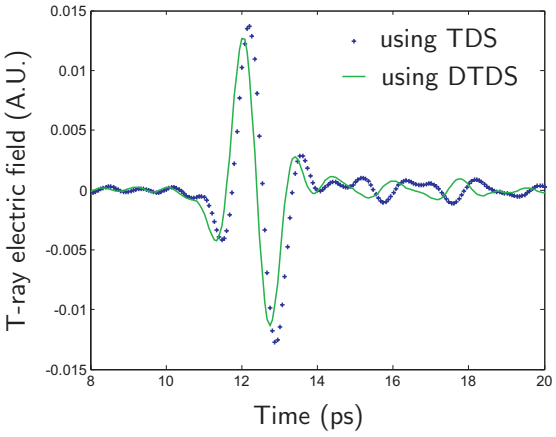

Figure 11. DTDS y_d and $(y_r - y_s)/2$. This graph compares the waveform from a liquid DTDS experiment, y_d (crosses), to the difference between two waveforms from normal TDS, $(y_r - y_s)/2$ (solid line). Apart from changing the modulation of the sample, exactly the same experimental conditions were used. The waveforms have been smoothed with a bandpass filter for clarity. The filter was set at the T-ray frequencies with highest SNR for this experiment, which were 0.2 to 1.2 THz. The close match of the two waveforms demonstrates the accuracy of liquid DTDS in characterising a material – the same results are achievable as with T-ray TDS, with potentially far less noise.

The biggest problem with this system was the inaccuracy in the displacement measurements. The error due to δd is far greater than the error due to δT. For example, Table 1 shows approximate error levels for a typical spectroscopy measurements. The greatest source of error comes from inaccuracies in the measurement of d. The mechanical displacement accuracy can be greatly increased using a number of methods, including real-time external displacement measurement and closed-loop control. One method of achieving a very low δd is to use a piezoelectric translation system, as discussed in Sec. 5.

4.4. Test of the error sources

The mismatch between the TDS and DTDS measurements in Fig. 11 was due to translation stage noise. The error in the parameters of interest (n and κ) introduced by the translation stage noise for DTDS is shown in Table 1. This table shows the prototype DTDS liquid sample modulator introduced a more mechanical noise, cancelling the reduced T-ray noise in DTDS. This problem is being addressed in ongoing work by using a sample holder will reduced mechanical error (see Sec. 5).

The mechanical errors were due to non-linearities in the sample modulator (displacement vs. voltage).[30] These non-linearities could be minimised by operating at an optimal frequency (10 Hz) and displacement (1.6

Table 1. Error sources in liquid DTDS. This Table compares the errors arising from the T-ray spectrometer (due to $\delta\tilde{T}$) and the thickness measurement (due to δd) as they contribute to the overall material parameter uncertainty (δn and $\delta\kappa$). For the spectral component at 0.5 THz, for example, the noise in the T-ray spectrum was measured to be $\delta\rho = 0.020$ and $\delta\phi = 0.037$. The signal level was given by $\rho = 0.67$ and $\phi = 22.30$. The thickness change d was 1.6 mm. The thickness accuracy was either $\delta d = 5$ μm for the manual translation state in normal TDS, or $\delta d = 0.1$ mm for the audio speaker in double-modulated DTDS. These results come from actual measurements of anhydrous dioxane. The error estimates are calculated using the equations in Sec. 2.2. This Table shows that the effect of both sources is approximately the same for the manual stage, but the error due to δd is much greater for the double-modulated DTDS measurement. As discussed in Sec. 2.2, the error due to δd can be reduced even further for the manual stage by using a thicker sample change (increase d from 1.6 mm), then $\delta\tilde{T}$ dominates. The error in $\delta\tilde{T}$ can conceivably be reduced through double-modulated DTDS, but unfortunately in this prototype, the noise due to δd is so great, the overall noise is higher.

Noise source	Parameter	Error ($\times 10^{-4}$)	Sample modulation
T-ray noise ($\delta\tilde{T}$)	δn	4.4	TDS
	$\delta\kappa$	2.5	TDS
Translation stage noise (δd)	δn	4.2	TDS
		83	DTDS
	$\delta\kappa$	0.075	TDS
		1.5	DTDS

mm), which however placed constraints on the improvements of DTDS: (i) the T-ray noise is reduced for higher modulation frequencies, and (ii) the effect of errors is reduced for larger modulation displacements. These limitations are being addressed in ongoing work (see Sec. 5).

5. CONCLUSION

The results in this paper demonstrate a novel implementation of double-modulated DTDS for liquid spectroscopy. The prototype system confirmed the accuracy of calculations to estimate the potential noise reduction achievable with this technique (Eq. (19)). Unfortunately the prototype system built introduced excessive mechanical noise at higher modulation frequencies and amplitudes.

In ongoing work the sample holder system is being implemented using a high-accuracy modulator. One option being explored is a piezoelectric driven window. The advantage of a piezoelectric modulator over an audio speaker is the extreme accuracy of movement, with $\delta d/d$ better than 10^{-4}.

ACKNOWLEDGMENTS

The authors would like to acknowledge the financial support of the US National Science Foundation, the US Army Research Office, and the Australian Research Council.

REFERENCES

1. J. T. Kindt and C. A. Schmuttenmaer, "Far-infrared dielectric properties of polar liquids probed by femtosecond terahertz pulse spectroscopy," *Journal of Physical Chemistry* **100**(24), pp. 10373–10379, 1996.
2. S. P. Mickan, K. S. Lee, T.-M. Lu, J. Munch, D. Abbott, and X.-C. Zhang, "Double modulated differential THz-TDS for thin film dielectric characterization," *Microelectronics Journal* (Elsevier) **33**(12), pp. 1033–1042, 2002.
3. S. P. Mickan, J. S. Dordick, J. Munch, D. Abbott, and X.-C. Zhang, "Pulsed THz protein spectroscopy in organic solvents," in *Conference on Lasers and Electro-Optics '02*, p. 640, IEEE LEOS & OSA, (Long Beach, CA, U.S.A.), 2002.
4. S. P. Mickan, J. S. Dordick, J. Munch, D. Abbott, and X.-C. Zhang, "Terahertz spectroscopy of bound water in nano suspensions," in *Proceedings of SPIE - Biomedical Applications of Micro- and Nanoengineering*, D. Nicolau and A. P. Lee, eds., **4937**, pp. 49–61, Melbourne, Australia, 2002.

5. D. von der Linde, "Characterization of the noise in continuously operating mode-locked lasers," *Applied Physics B: Photophysics and Laser Chemistry* **39**(4), pp. 201–217, 1986.
6. E. Zoidis, M. Besnard, and J. Yarwood, "Far infrared spectroscopic studies of the molecular dynamics and interactions of pyridine in organic solvents," *Chemical Physics Letters* **203**, pp. 233–243, 1996.
7. C. Rønne, L. Thrane, P.-O. Åstrand, A. Wallqvist, K. V. Mikkelsen, and S. R. Keiding, "Investigation of the temperature dependence of dielectric relaxation in liquid water by THz reflection spectroscopy and molecular dynamics simulation," *Journal of Chemical Physics* **107**(14), pp. 5319–5331, 1997.
8. C. Rønne, K. Jensby, B. J. Loughnane, J. Fourkas, O. F. Nielsen, and S. R. Keiding, "Temperature dependence of the dielectric function of C_6H_6(l) and $C_6H_5CH_3$(l) measured with THz spectroscopy," *Journal of Chemical Physics* **113**(9), pp. 3749–3756, 2000.
9. D. S. Venables, A. Chiu, and C. A. Schmuttenmaer, "Structure and dynamics of nonaqueous mixtures of dipolar liquids. I. Infrared and far-infrared spectroscopy," *Journal of Chemical Physics* **113**(8), pp. 3243–3248, 2000.
10. M. L. T. Asaki, A. Redondo, T. A. Zawodzinski, and A. J. Taylor, "Dielectric relaxation of electrolyte solutions using terahertz transmission spectroscopy," *Journal of Chemical Physics* **116**(19), pp. 8469–8482, 2002.
11. L. Thrane, R. H. Jacobsen, P. U. Jepsen, and S. R. Keiding, "THz reflection spectroscopy of liquid water," *Chemical Physics Letters* **240**, pp. 330–333, 1995.
12. C. Rønne and S. R. Keiding, "THz reflection spectroscopy of H_2O(l) and D_2O(l)," in *Ultrafast Phenomena XI*, T. Elsaesser, J. G. Fujumoto, D. A. Wiersma, and W. Zinth, eds., *Springer Series in Chemical Physics* **63**, pp. 568–570, Springer-Verlag, Berlin, 1998.
13. I. H. Libon, M. Hempel, S. Seitz, N. E. Hecker, J. Feldmann, A. Hayd, G. Zundela, D. Mittleman, and M. Koch, "THz spectroscopy of polar liquids," in *Proceedings of SPIE - Terahertz Spectroscopy and Applications*, **3617**, pp. 24–29, (San Jose, CA, U.S.A.), 1999.
14. J. E. Pedersen and S. R. Keiding, "THz time-domain spectroscopy of nonpolar liquids," *IEEE Journal of Quantum Electronics* **28**(10), pp. 2518–2522, 1992.
15. M. C. Beard, G. M. Turner, D. S. Venables, and C. A. Schmuttenmaer, "Two-dimensional time-resolved THz spectroscopy of solvent response to photoexcitation," in *Trends in Optics and Photonics. Twelfth International Conference on Ultrafast Phenomena*, **43**, pp. 592–594, OSA, (Charleston S.C. USA), 2000.
16. M. C. Beard and C. A. Schmuttenmaer, "Using the finite-difference time-domain pulse propagation method to simulate time-resolved THz experiments," *Journal of Chemical Physics* **114**(7), pp. 2903–2909, 2001.
17. D. S. Venables and C. A. Schmuttenmaer, "Time-resolved THz studies of liquid dynamics," in *Ultrafast Phenomena XI*, T. Elsaesser, J. G. Fujumoto, D. A. Wiersma, and W. Zinth, eds., *Springer Series in Chemical Physics* **63**, pp. 565–567, Springer-Verlag, Berlin, 1998.
18. D. S. Venables and C. A. Schmuttenmaer, "Spectroscopy and dynamics of mixtures of water with acetone, acetonitrile, and methanol," *Journal of Chemical Physics* **113**(24), pp. 11222–11236, 2000.
19. D. S. Venables and C. A. Schmuttenmaer, "Structure and dynamics of nonaqueous mixtures of dipolar liquids. II. Molecular dynamics simulations," *Journal of Chemical Physics* **113**(8), pp. 3249–3260, 2000.
20. S. P. Mickan, J. Xu, T. Yuan, J. Munch, D. Abbott, and X.-C. Zhang, "The limits of time-domain THz spectral resolution," in *Proceedings of SPIE - Photonics: Design, Technology, and Packaging*, C. Jagadish et al., ed., **5277**, p. In Press, SPIE, 2003.
21. M. Born and E. Wolf, *Principles of Optics*, Cambridge University Press, 6th ed., 1997.
22. L. Duvillaret, F. Garet, and J.-L. Coutaz, "A reliable method for extraction of material parameters in terahertz time-domain spectroscopy," *IEEE Journal of Selected Topics in Quantum Electronics* **2**(3), pp. 739–746, 1996.
23. L. Duvillaret, F. Garet, and J.-L. Coutaz, "Highly precise determination of optical constants and sample thickness in terahertz time-domain spectroscopy," *Applied Optics* **38**(2), pp. 409–415, 1999.
24. G. Arjavalingam, Y. Pastol, J.-M. Halbout, and G. V. Kopcsay, "Broad-band microwave measurements with transient radiation from optoelectronically pulsed antennas," *IEEE Transactions on Microwave Theory and Techniques* **38**(5), pp. 615–621, 1990.

25. S. P. Mickan, A. Menikh, H. Liu, C. A. Mannella, R. MacColl, D. Abbott, J. Munch, and X.-C. Zhang, "Label-free bioaffinity detection using terahertz technology," *Physics in Medicine and Biology* **47**(21), pp. 3789–3796, 2002.
26. L. Duvillaret, F. Garet, and J. L. Coutaz, "Influence of noise on the characterization of materials by terahertz time-domain spectroscopy," *Journal of the Optical Society of America B: Optical Physics* **17**(3), pp. 452–461, 2000.
27. S. P. Mickan, D. Abbott, J. Munch, and X. C. Zhang, "Noise reduction in terahertz thin film measurements using a double modulated differential technique," *Fluctuation and Noise Letters* **2**(1), pp. 13–29, 2002.
28. D. Lohse, "Bubble puzzles," *Physics Today* **56**(2), pp. 36–41, 2003.
29. S. P. Mickan and X.-C. Zhang, "T-ray sensing and imaging," in *Terahertz Sensing Technology: Electronic Devices & Advanced Technology*, D. Woolard, M. S. Shur, and W. Leorop, eds., *Selected Topics in Electronics and Systems*, ch. 8, pp. 251–326, World Scientific Publishing Company, 2003.
30. S. P. Mickan, R. Shvartsman, D. Abbott, J. Munch, and X. C. Zhang, "Noise reduction in dual-thickness laser-based T-ray material characterization," in *Proceedings of SPIE - Fluctuations and Noise in Photonics and Quantum Optics*, D. Abbott, J. Shapiro, and Y. Yamamoto, eds., **5111**, pp. 198–213, SPIE, Washington, DC, U.S.A., 2003.